Overview of KSTAR initial operation

2011 Nucl. Fusion 51 094006

Nucl. Fusion **51** (2011) 094006 (12pp) doi:10.1088/0029-5515/51/9/094006

Overview of KSTAR initial operation

M. Kwon, Y.K. Oh, H.L. Yang, H.K. Na, Y.S. Kim, J.G. Kwak, W.C. Kim, J.Y. Kim, J.W. Ahn[9], Y.S. Bae, S.H. Baek, J.G. Bak, E.N. Bang, C.S. Chang[4], D.H. Chang[1], I. Chavdarovski, Z.Y. Chen, K.W. Cho, M.H. Cho[3], W. Choe[4], J.H. Choi, Y. Chu, K.S. Chung[5], P. Diamond[8], H.J. Do, N. Eidietis[11], A.C. England, L. Grisham[10], T.S. Hahm[10], S.H. Hahn, W.S. Han, T. Hatae[14], D. Hillis[9], J.S. Hong, S.H. Hong, S.R. Hong, D. Humphrey[11], Y.S. Hwang[2], A. Hyatt[11], Y.K. In[13], G.L. Jackson[11], Y.B. Jang, Y.M. Jeon, J.I. Jeong, N.Y. Jeong, S.H. Jeong[1], H.G. Jhang, J.K. Jin, M. Joung, J. Ju, K. Kawahata[15], C.H. Kim, D.H. Kim[2], Hee-Su Kim, H.S. Kim[2], H.K. Kim, H.T. Kim, J.H. Kim, J.C. Kim, Jong-Su Kim, Jung-Su Kim, Kyung-Min Kim, K.M. Kim[2], K.P. Kim, M.K. Kim, S.H. Kim[1], S.S. Kim, S.T. Kim, S.W. Kim, Y.J. Kim, Y.K. Kim[5], Y.O. Kim, W.H. Ko, Y. Kogi[16], J.D. Kong, S. Kubo[15], R. Kumazawa[15], S.W. Kwak, J.M. Kwon, O.J. Kwon[6], M. LeConte, D.G. Lee, D.K. Lee, D.R. Lee, D.S. Lee, H.J. Lee, J.H. Lee, K.D. Lee, K.S. Lee, S.G. Lee, S.H. Lee[4], S.I. Lee, S.M. Lee, T.G. Lee, W.C. Lee[3], W.L. Lee, J. Leur[11], D.S. Lim, J. Lohr[11], A. Mase[18], D. Mueller[10], K.M. Moon, T. Mutoh[15], Y.S. Na[2], Y. Nagayama[15], Y.U. Nam, W. Namkung[3], B.H. Oh[1], S.G. Oh[7], S.T. Oh, B.H. Park, D.S. Park, H. Park[3], H.T. Park, J.K. Park[10], J.S. Park, K.R. Park, M.K. Park, S.H. Park, S.I. Park, Y.M. Park, Y.S. Park[12], B. Patterson[15], S. Sabbagh[12], K. Saito[15], S. Sajjad, K. Sakamoto[14], D.C. Seo, S.H. Seo, J.C. Seol, Y. Shi[18], N.H. Song, H.J. Sun, L. Terzolo, M. Walker[11], S.J. Wang[1], K. Watanabe[14], A.S. Welander[11], H.J. Woo[5], I.S. Woo, M. Yagi[17], Y. Yaowei, Y. Yonekawa, K.I. Yoo, J.W. Yoo, G.S. Yoon[3], S.W. Yoon and the KSTAR Team

National Fusion Research Institute, Daejeon, Korea
[1] Korea Atomic Energy Research Institute, Daejeon, Korea
[2] Seoul National University, Seoul, Korea
[3] Pohang University of Science and Technology, Pohang, Korea
[4] Korea Advanced Institute of Science and Technology, Daejeon, Korea
[5] Hanyang University, Seoul, Korea
[6] Daegu University, Daegu, Korea
[7] Ajou University, Sawon, Kyonggi, Korea
[8] University of San Diego, San Diego, CA, USA
[9] Oak Ridge National Laboratory, Oak Ridge, TN, USA
[10] Princeton Plasma Physics Laboratory, Princeton, NJ, USA
[11] General Atomics, San Diego, CA, USA
[12] Columbia University, New York, NY, USA
[13] Fartech, San Diego, CA, USA
[14] Japan Atomic Energy Agency, Naka, Ibaraki, Japan
[15] National Institute of Fusion Science, Toki, Gifu, Japan
[16] Fukuoka Institute of Technology, Fukuoka, Japan
[17] Kyushu University, Fukuoka, Japan
[18] Institute of Plasma Physics of Academia Sinica, Hefei, Anhui, People's Republic of China

E-mail: kwonm@nfri.re.kr

Received 31 December 2010, accepted for publication 26 May 2011
Published 31 August 2011
Online at stacks.iop.org/NF/51/094006

Abstract
Since the successful first plasma generation in the middle of 2008, three experimental campaigns were successfully made for the KSTAR device, accompanied with a necessary upgrade in the power supply, heating, wall-conditioning and diagnostic systems. KSTAR was operated with the toroidal magnetic field up to 3.6 T and the circular and shaped plasmas with current up to 700 kA and pulse length of 7 s, have been achieved with limited capacity of PF magnet power supplies.

The mission of the KSTAR experimental program is to achieve steady-state operations with high performance plasmas relevant to ITER and future reactors. The first phase (2008–2012) of operation of KSTAR is dedicated to the development of operational capabilities for a super-conducting device with relatively short pulse. Development of start-up scenario for a super-conducting tokamak and the understanding of magnetic field errors on start-up are one of the important issues to be resolved. Some specific operation techniques for a super-conducting device are also developed and tested. The second harmonic pre-ionization with 84 and 110 GHz gyrotrons is an example. Various parameters have been scanned to optimize the pre-ionization. Another example is the ICRF wall conditioning (ICWC), which was routinely applied during the shot to shot interval.

The plasma operation window has been extended in terms of plasma beta and stability boundary. The achievement of high confinement mode was made in the last campaign with the first neutral beam injector and good wall conditioning. Plasma control has been applied in shape and position control and now a preliminary kinetic control scheme is being applied including plasma current and density. Advanced control schemes will be developed and tested in future operations including active profiles, heating and current drives and control coil-driven magnetic perturbation.

(Some figures in this article are in colour only in the electronic version)

1. Introduction

The Korea Superconducting Tokamak Advanced Researches (KSTAR) successfully completed the first plasma generation in the middle of 2008, and entered into the initial operation phase from 2009 [1]. In this paper, we will present highlights of the major results of the research experiments and upgrade activities for the last three campaigns.

The KSTAR device is a medium-size, D-shaped tokamak with the major machine parameters of $R = 1.8$ m, $a = 0.5$ m, $B = 3.5$ T, $I_p = 2$ MA, $\kappa_x = 2.0$ and $\delta_x = 0.8$. Its main research goal is to demonstrate the steady-state operation in the high-performance, advanced tokamak (AT) modes and KSTAR adopted several advanced features to support this goal, which include a fully superconducting magnet system, flexible heating and current-drive (CD) systems with long-pulse operation capability, strong plasma shaping capability with a conducting wall close to plasmas and advanced diagnostics and control systems. With these features, KSTAR has been designed to play a significant role as a new device capable of addressing many scientific and technical issues, critical for the development of steady-state, high-performance operation scenarios related to ITER and DEMO reactors.

From the core physics point of view, 'steady-state operation' is defined for tokamaks as 'a discharge duration longer than several current diffusion time τ_R (10^{-1} to a few tens of seconds depending on the present devices) to reach constant loop-voltage condition' [2]. Comparing τ_R with typical characteristic time of technological aspects of tokamak operations, necessity of the long-pulse operation is shown clearly: $\sim$10 s to the thermal equilibrium of the plasma facing components (PFCs), $\sim$100 s to the wall saturation time, $\sim 10^6$ s for the lifetime of PFCs. This simple comparison gives issues that should be considered for steady-state operation: the sustainment of magnetic configuration by superconducting coils and non-inductive current drive systems, the real-time control of kinetic configuration including pressure, rotation and particle content, and the reliable operation of superconducting magnets, heating and current drive systems, PFCs and diagnostics. Describing briefly some of such issues and the possible KSTAR role, KSTAR has been designed to play a key role as a test-bed of the ITER superconducting magnet system, which is made of the same material, Nb_3Sn, as for KSTAR. KSTAR will provide rich experiences of the operation characteristics, including the effect of ac-loss of the superconducting magnets which is the energy dissipation caused by time-varying magnetic field, transport current or both, of the PF coil system and the He refrigerator and of the operation skills to avoid the quench with maximum efficiency. The optimum scenario for a full non-inductive current drive will also be explored in KSTAR, using its flexible heating and CD systems which include NBI, ICRH/FWCD, LHCD and ECH/ECCD. Particularly, we will try to maximize the bootstrap current fraction with a good alignment, which is a critical element required to achieve the AT modes. A significant effort will also be put on the development of an advanced divertor system, which can withstand the long-pulse operation in the high power-density condition, expected in AT modes. The control of particles and impurity is also an important issue for the steady-state operation, and an intensive study will be performed on the subjects, such as wall recycling, saturation, retention, erosion and dust particles. To achieve the disruption-free long-pulse operation of high-beta plasma, it is also critical to develop a robust active control capability of various MHD instabilities, which include the locked-mode, NTM, ELM and RWM. We will try to develop this capability utilizing the in-vessel control coil (IVCC), pellet injector system and other actuators such as the ECCD system in KSTAR. A substantial effort will be made for the control of plasma transport and profiles, such

as the plasma current, density, temperature profiles and local transport barriers. Utilizing the advanced diagnostics and control systems, and also the long-pulse operation capability, the plasma profile will be detected and adjusted in real time for the realization of optimum target profiles, required for the AT mode of operation.

In order to address the research issues and to achieve the research goal described above, it is now planned that KSTAR will be gradually upgraded in operations and the ancillary systems such as heating and CD systems. It should be noted that our basic strategy is to develop the steady-state, high-performance operation scenarios in the relatively low or medium power-density regime for the first-half of the operation period till 2018, aiming at supporting more ITER-relevant researches, and then upgrading the scenarios to the high power-density regime to support the advanced DEMO-relevant researches in the later half.

The main research goals up to the third campaign are to achieve the D-shape plasma with the position and shape control using the IVCC and PF coils, and then perform relevant physics studies at ohmic and L-mode plasmas with the initial heating power from NBI, ICRH and ECH systems. Robust target plasmas with strong shaping ($\kappa_x = 1.9$ and $\delta_x = 0.8$) at medium plasma current of about 0.7 MA were routinely obtained and H-mode transition was observed with marginal heating power.

Table 1. KSTAR technical specifications and achieved parameters.

PARAMETERS	Designed	Achieved
Major radius, R_0	1.8 m	1.8 m
Minor radius, a	0.5 m	0.5 m
Elongation, κ	2.0	1.9
Triangularity, δ	0.8	0.8
Plasma volume	17.8 m^3	17.8 m^3
Bootstrap Current, f_{bs}	> 0.7	-
PFC Materials	C, CFC (W)	C
Plasma shape	DN, SN	DN
Plasma current, I_p	2.0 MA	0.7 MA
Toroidal field, B_0	3.5 T	3.6 T
Pulse length	300 s	7 s
β_N	5.0	> 1.0
Plasma fuel	H, D	H, D, He
Superconductor	Nb_3Sn, NbTi	Nb_3Sn, NbTi
Auxiliary heating /CD	~ 28 MW	2.0 MW
Cryogenic	9 kW @4.5K	5 kW @4.5 K

2. Device updates

After completion of the construction in the middle of 2007, KSTAR has been continuously upgraded with important systems, removing a major limit on the studies for the steady-state operations.

Just before the third campaign of KSTAR, many in-vessel components such as inboard limiters, divertors, passive stabilizers, IVCCs, in-vessel cryo-pumps (IVCP) and various diagnostic systems have been newly installed, suitable for up to 20 s long-pulse operation. Vacuum vessel and pumping duct were baked at a temperature of 130 °C and PFCs at 225 °C (capable up to 350 °C) by hot nitrogen gas. Boronization in KSTAR uses carborane solid powder ($C_2B_{10}H_{12}$) [3] and it was successfully applied showing that the water and oxygen impurities were effectively removed. The glow discharge cleaning (GDC) is also a good method to control wall pumping. Before the campaign, D_2 gas is normally used for chemical cleaning of the wall impurities followed by He GDC for reducing the wall retention of the D_2 gas. During the campaign, only He gas is used for GDC. For a machine equipped with superconducting coils, ICRH or ECRH wall conditioning (ICWC or ECWC) would be a mandatory choice. Wall conditioning with ICWC between shots is performed regularly to have a better wall condition and density control [4]. Table 1 tabulates the technical specifications and the current achievements of KSTAR, actively preparing for its long-pulse mission step by step to become one of the promising candidates for ITER pilot devices.

The ac-loss of superconducting magnet systems is an important issue for the steady-state operation of tokamaks such as KSTAR and ITER. In KSTAR, the ac-loss might cause the temperature increase in the liquid helium up to the limit which could endanger a safe operation of the poloidal field (PF) magnets. Characteristics of ac magnets in KSTAR have been measured and symptoms leading the liquid-He temperature close to the quench limit have been observed for certain cases. Remedies have been sought and tested including the flow-rate increase and control of current-ramp rate [5].

2.1. Plasma facing components

As shown in figure 1, the KSTAR PFCs consists of inboard limiter, divertor, passive stabilizer, poloidal limiter and two sets of NB protection armor. The heat-sink plate of the inboard limiter has a toroidally continuous cylinder-shape, which are made of stainless steel (SS316LN) with internal cooling channels for active water cooling and baking. The plate is installed on the straight section of the vacuum vessel, and is covered by graphite tiles that are simply mounted on the plate by bolts. A total of 16 sub-segments of the inboard limiter are covered by graphite tiles, however, before the long-pulse operation starts, four sub-segments will be replaced with carbon-fibre-composite (CFC) tiles, on which energetic neutral beam strikes and strong heat influx takes place.

The divertor system consists of inboard, central and outboard parts. Each part contains eight heat-sink plates that locate in the upper and lower side of the vacuum vessel with up-down symmetry for double-null (DN) operation. The entire area of the heat-sink plates is covered with graphite tiles but eventually with CFC tiles by bolts to withstand high temperature (maximum 1200 °C) at striking points for the case of maximum heat influx of 4.3 MW m^{-2} expected for 16 MW of auxiliary heating power.

The passive stabilizer will play a role on both plasma position control and on suppression of MHD instabilities through various combinations with active control coils. Two

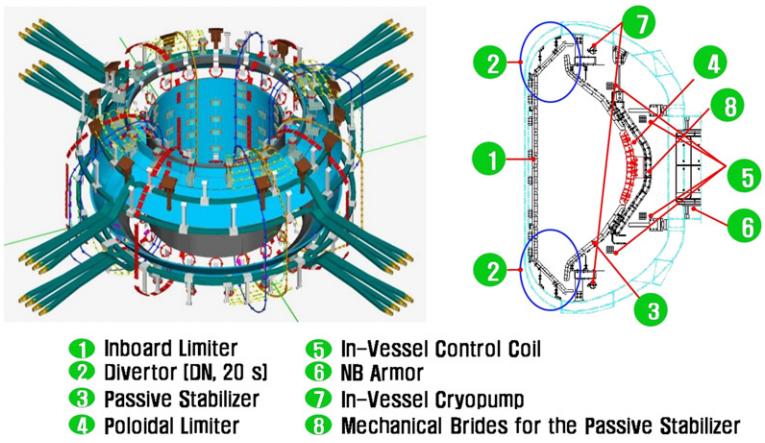

Figure 1. Configuration of KSTAR in-vessel components.

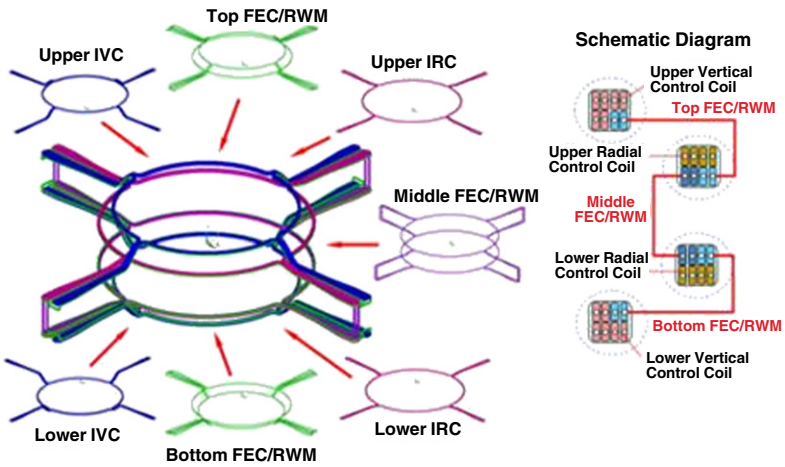

Figure 2. Electrical connection scheme of the IVCC.

toroidal ring-shaped copper plates made of CuCrZr alloy have up-down symmetry. Each plate is electrically segmented into four quadrants, and a quadrant is electrically connected to an adjacent quadrant by 'gap resistors' to adjust the total resistance of the passive plate in the toroidal direction. The design was optimized through a trade-off study between the controllability of the $n = 1$, resistive-wall mode (RWM) and the controllability of vertical instability by the IVCC. For improving the penetration of magnetic field induced by the IVCC, the number of gap resistors increased to four but this change did not degrade much the suppression capability of $n = 1$, RWM [6]. The poloidal limiter comprises three D-shaped strings to protect launchers of the ICRF and the LHCD.

2.2. In-vessel control coil

The IVCC system was developed to take advantage of the active control of the plasma position, the field error correction (FEC) and the RWM [7, 8]. More recently, the IVCC is expected to be effectively utilized in suppression of the edge-localized mode (ELM) [6, 9] by changing its electrical connection. This important system adopted a unique concept of segmented coil assembly, having 16 segments and their support structures [10]. Each segment contains eight water-cooled normal copper conductors that are partially connected to an adjacent segment in series to form four circular coils for position control as shown in figure 2, while the remaining copper conductors are connected to the vertically neighbouring segment to form twelve 'picture-frame' coils for the FEC and RWM control. The eight copper conductors in a segment are encapsulated by a 3 mm thick jacket made of stainless steel (SS316LN).

2.3. Neutral beam injection system

The first neutral beam injection (NBI) system has been constructed to deliver more than 1 MW of deuterium neutral beam in the 2010 campaign of KSTAR. Among the various key components of the NBI, a bucket-type positive ion source has demonstrated 55 A of a hydrogen ion beam at 100 keV with 2 s in the beam pulse [11]. The source also achieved 300 s in the beam pulse length with 33 A at 90 keV for long-pulsed operations. More recently, the source was substantially modified by replacing the plasma generator by a new one, developed by the Japan Atomic Energy Agency (JAEA). The procedure of the ion source conditioning was started from the filament heating, then moved to the high voltage insulation test at the grid. Then the high voltage was applied to the

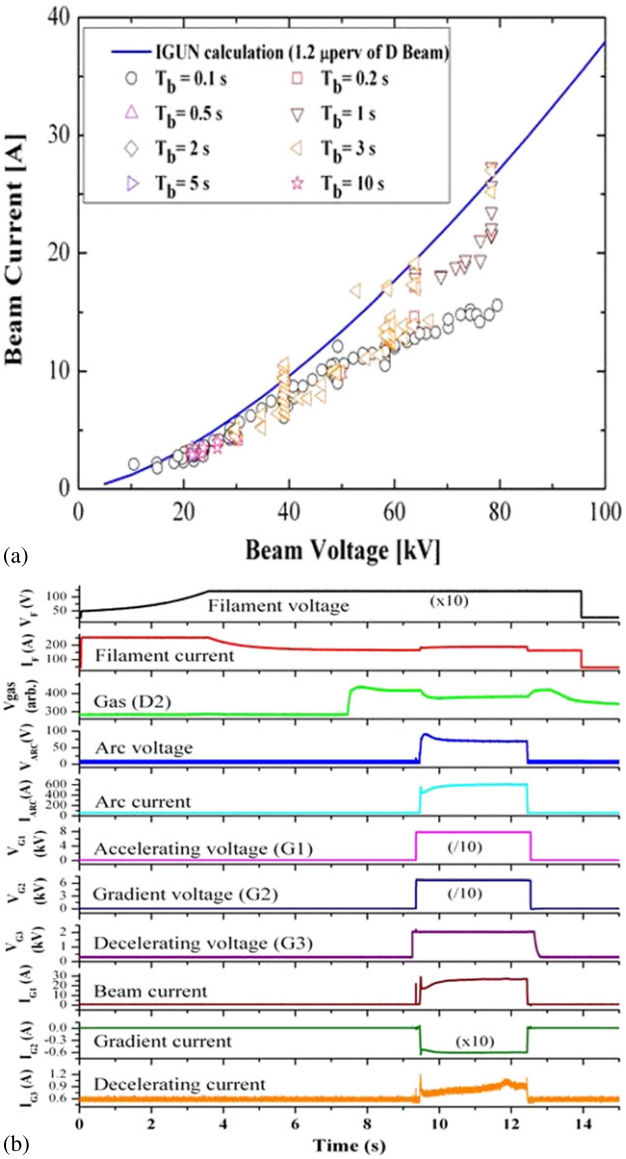

Figure 3. (*a*) The beam perveance data and (*b*) the waveforms of the 10-s beam extraction with the beam energy of 100 keV and the beam current of 41 A. The filament voltage and current are those of the filament no 3.

accelerating grid up to 82 kV and the decelerating grid up to −2 kV with a maximum pulse duration of 30 s.

As continuous conditioning of the ion source was implemented, the beam extraction experiments finally achieved 100 keV and 41 A in maximum beam energy and ion beam current for 10 s, respectively. Figure 3 shows the beam extraction results. The optimum arc power is investigated to obtain the beam perveance close to the designed value of 1.2 μ-perveance as the accelerating beam voltage increases. The waveforms of voltage and current at the filament and arc power supplies, the accelerating power supply and the decelerating power supply are also shown in figure 3. Moreover, more than 1.2 MW of NBI at 85 keV of the beam energy has been successfully demonstrated in the 2010 campaign, which has decisively contributed to the first achievement of H-mode in KSTAR. This successful achievement in the NB experiment in the 2010 campaign

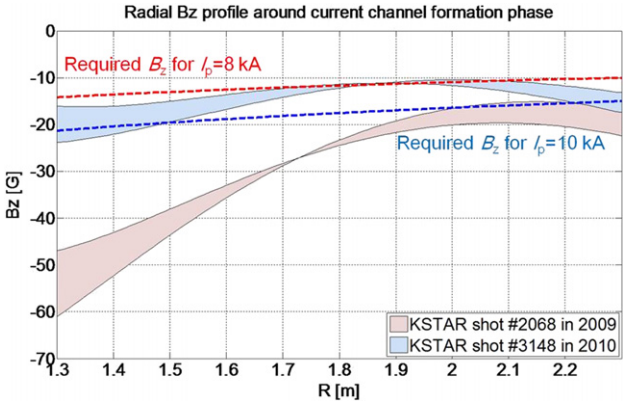

Figure 4. The effect of Incoloy on the field-null is clearly shown in the simulation. The gradient of B_z near the field-null centre is changed by the influence of Incoloy. The correction was done by adding the proper amounts of vertical field to the startup scenario.

promises the possibility of the focused H-mode experiment in the next year with more than 2 MW of power through system optimization.

2.4. ECH/ECCD and LHCD systems

Success in the ECH-assisted startup using the second harmonic [12] EC wave is expected to provide lots of crucial techniques for reliable startup with relatively low loop voltage (∼3 V) in superconducting tokamak devices. The KSTAR ECH-assisted startup system originally utilized 84 GHz gyrotron with a capability of 500 kW and 2 s pulse length. As a backup, another system was prepared with a 110 GHz, diode-gun type gyrotron without a depressed collector, which can provide 800 kW for 2 s pulse length and 500 kW for 5 s pulse length. The 110 GHz system was used for the second harmonic EC heating at the toroidal magnetic field of 2 T. This additional tube could provide a wider operation window in ECCD as well as better security for plasma startup.

A 5 GHz LHCD system that uses the same frequency for the proposed ITER system [13] will play a key role in providing plasma current and in controlling its profile. To investigate the issues of steady-state operations, the first LHCD system is scheduled to be installed in 2012 using the prototype of 5 GHz, 500 kW CW klystron and the un-cooled, fully active, phased-array, waveguide launcher. The launcher is made up of two arrays, each with eight waveguides in a column with consideration of the power upgrade to 1 MW [14]. For injection of the 5 GHz LH wave into the plasma, an LH launcher was designed based on the four-way splitter without active water cooling.

3. Recent experimental results

3.1. Plasma startup and control

The startup of the KSTAR device differs from typical tokamak startup in two aspects. First of all, the KSTAR device requires a blip resistor insertion system (BRIS) to produce sufficient change in PF coil current during the initial stage of discharge due to limited voltage capability of PF power supplies. When the currents in the central solenoids are discharged fast using

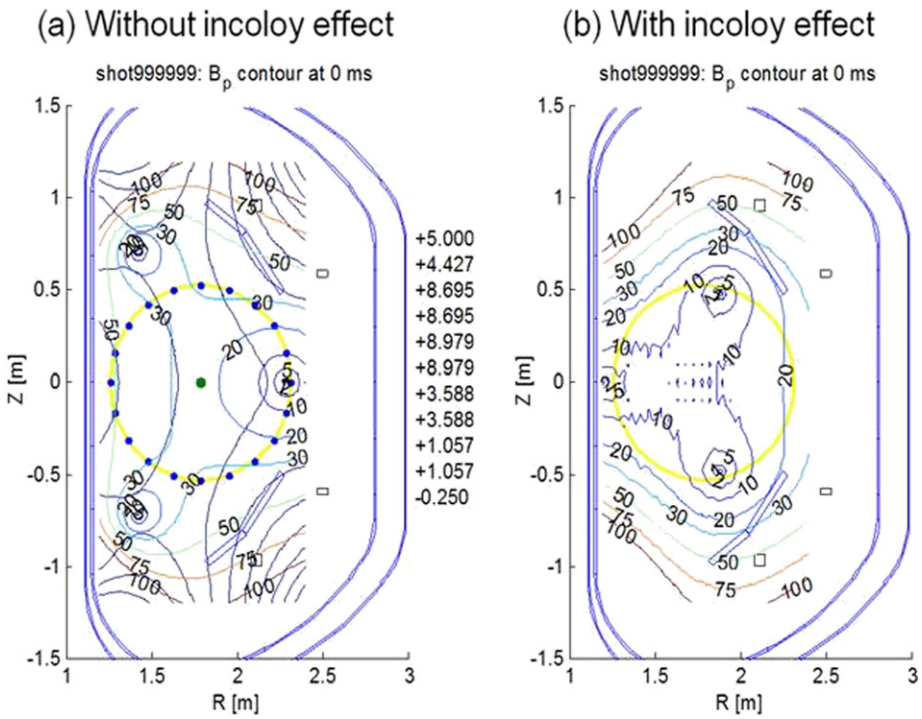

Figure 5. Magnetic field configuration with and without compensation of Incoloy effect.

the BRIS, it is required to provide the necessary vertical field for radial position control during the initial plasma current ramp-up phase. The required fast varying vertical field is also generated by the BRIS in the outer coils with significant initial charging even though the magnetic field generated by those coils degrades initial field-null quality [15]. This complicates the startup of the KSTAR device due to the short connection length of the charged particles to the wall

The other unconventional aspect of KSTAR startup originates from the ferromagnetic material, Incoloy 908 used in the PF and toroidal field (TF) coils. The impact of this was quite serious during the startup phase. Roughly Incoloy is generating approximately −20 G vertical field at the field-null centre and its inclusion in the startup scenario development is important for the successful startup in KSTAR [16, 17]. Based on the FEM analysis of the Incoloy effect, it was determined that the effect of Incoloy on the startup was not trivial. As shown in figure 4, due to a strong impact from Incoloy in the central solenoids, the radial profile is completely different from the case without Incoloy. Consequently, not only does it degrade the initial field-null quality but the positional stability of the initial plasma column can be affected by the modified field gradient from Incoloy. Therefore a simple offset correction for Incoloy impact is just partially effective. The field decay index, $n = -(\mathrm{d}B_R/\mathrm{d}z)/(B_z/R)$, has a negative value for vertically unstable plasma and a positive value larger than 1.5 for radially unstable plasma. Thus, the stable plasma should have a positive index value ranged from 0 to 1.5.

Systematic efforts are being conducted to establish robust startup scenarios with compensation of the aforementioned effects of ferromagnetic materials. When the Incoloy effect is added to the startup scenario correctly, field structure in figure 5(*a*) is transformed to field-null structure as shown in figure 5(*b*). As a result, the degraded field null was improved

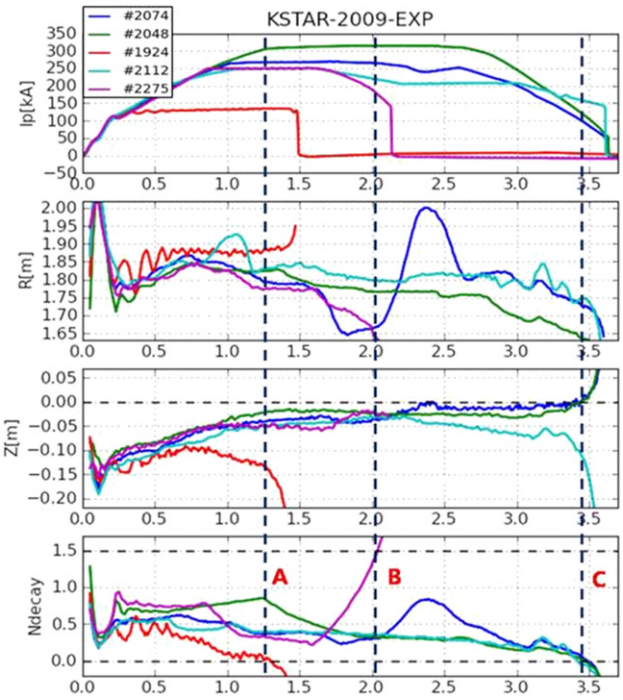

Figure 6. Basic stability analysis of KSTAR 2009 plasmas. According to the decay index of magnetic field, it clearly show that shot 2275 was terminated by RDE and the others by VDE.

and the resulting decay index became the value which satisfies the stability in both radial and vertical directions. Knowledge obtained from these expedites with the magnetic materials can be applicable to the ITER startup since there will be a considerable amount of ferritic materials around the main tokamak structure in ITER [19].

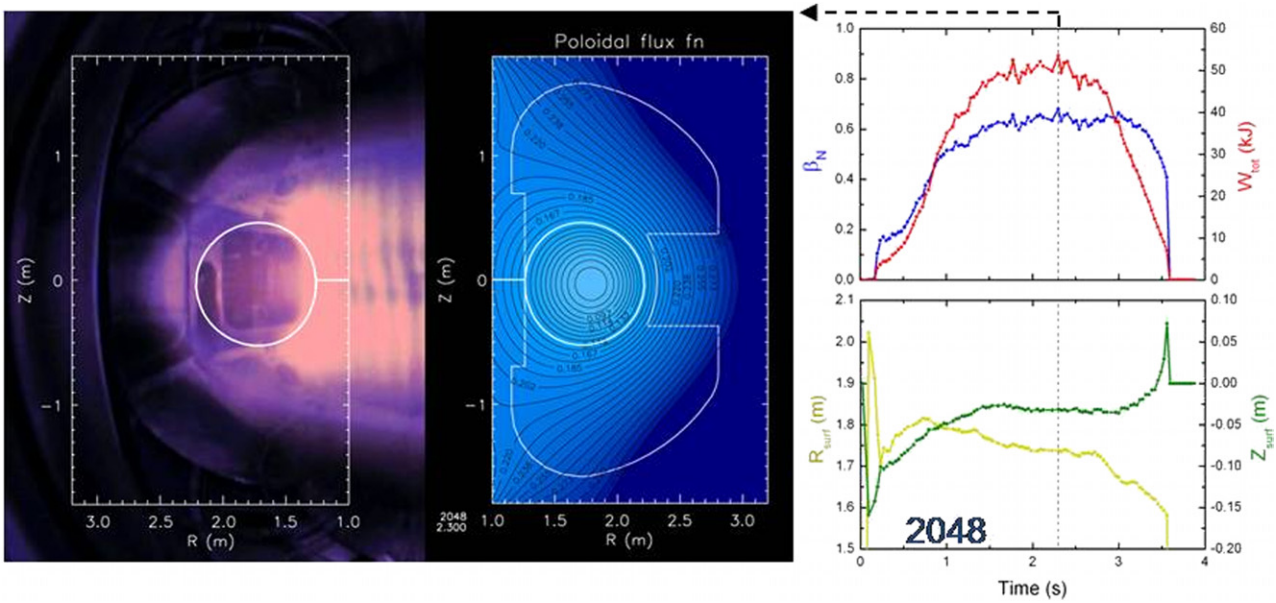

Figure 7. CCD images and EFIT comparison for shot 2048.

Figure 6 shows results of basic stability analysis [18] for several representative shots in the KSTAR 2009 campaign. The field decay index was calculated at the effective centre of plasma column with reconstructed magnetic fields excluding plasma contributions. As shown in the figure, the field decay index of shot 2275 exceeded 1.5, so that the discharge was terminated after that time point by radial displacement event (RDE). Contrarily other shots such as 1924, 2048, 2074 and 2112 show that the field decay index became negative around the time points of A and C, so that those shots were terminated by vertical displacement event (VDE).

The equilibrium reconstruction was done with EFIT as shown in figure 7 and it also showed the evolution of the stored energy and the beta value [6]. Figure 7 clearly shows a downward-shifted plasma column. This downshift of plasma column, particularly during the ramp-up phase, suggests existence of a certain level of the radial magnetic field (B_r) at the midplane so that the potential sources of B_r are also investigated. It turns out that the eddy current flowing in the up-down asymmetric cryostat structure may provide the required B_r for the downshift. When cryostat is included in the FEM model, the simulated voltage is in better agreement with the measured one by flux loops and it suggests that the effect of cryostat is not trivial and its effect is larger on the outer flux loops installed in an up-down symmetrical way. However, this up-down asymmetry were well controlled in the 2010 campaign by either B_r compensation using a slow up-down paired shaping coil or fast vertical stabilization using an IVC coil.

3.2. Second harmonic ECH pre-ionization

The second harmonic electron cyclotron heating (ECH)-assisted startup has been established to provide the reliable plasma startup with low toroidal loop voltage in KSTAR. For the 2008 first plasma campaign, the KSTAR was operated with toroidal magnetic field of 1.5 T at the major radius of 1.7 m

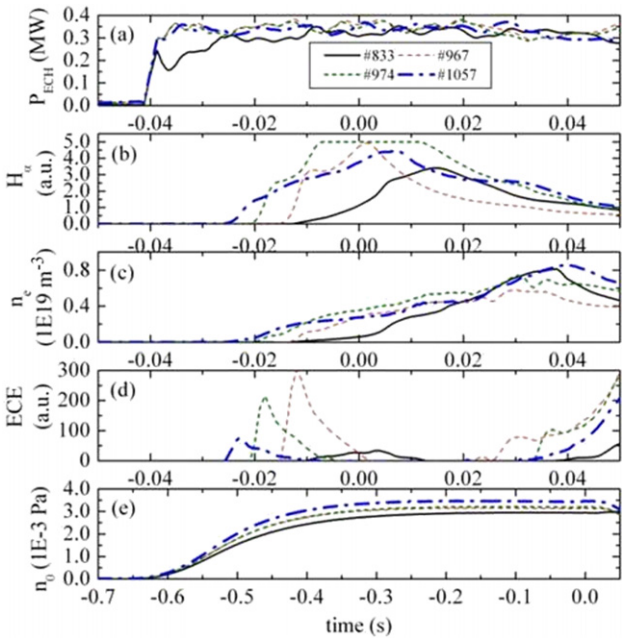

Figure 8. Typical 84 GHz second harmonic ECH pre-ionization experimental results for different beam launching angles.

which corresponded to the second harmonic resonant field with a 84 GHz EC wave.

The experimental results showed the feasibility of the second harmonic ECH-assisted startup with the low loop voltage ranged from 2 V (0.24 V m^{-1}) to 3 V (0.36 V m^{-1}) [12]. The application of the EC beam before the onset of the inductive toroidal electric field provided a localized plasma confined by the poloidal magnetic field-null structure which was obtained by the initial magnetization in seven pairs of the PF coils. It also allowed the burn-through and sustained the plasma during the current ramp-up. The optimized condition of ECH pre-ionization was investigated with parameter scans

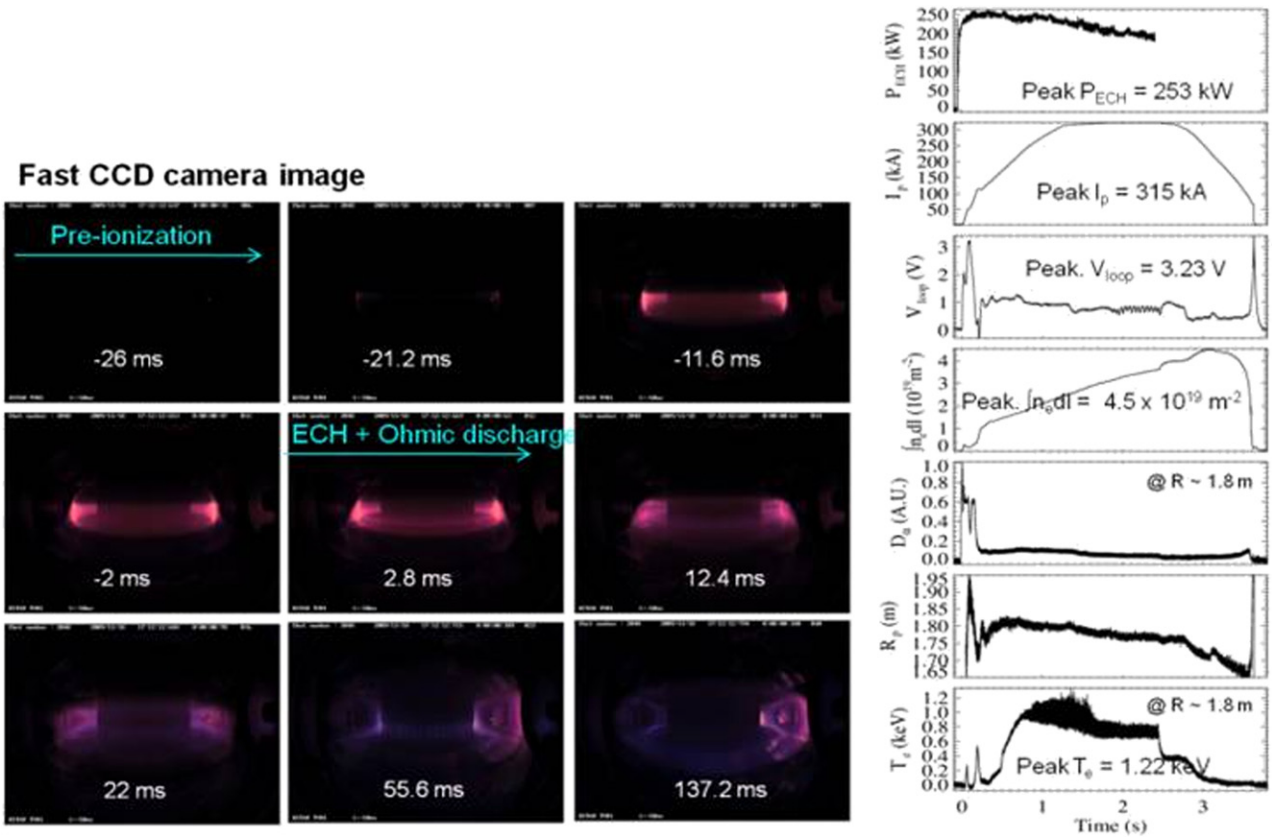

Figure 9. The 110 GHz second harmonic ECH-assisted startup in the 2009 campaign with snapshots of the CCD-pictured plasmas.

of hydrogen and deuterium pre-fill gas pressure, resonance position, polarization and vertical magnetic field without ohmic discharge. The pre-ionization was very efficient at the higher pre-fill gas pressure and the oblique beam injection crossing the resonance position. The oblique injection angle of 15° was the best condition to provide the reliable ECH-assisted startup as shown in figure 8. The pre-ionization was delayed at the low pre-fill pressure, the inboard resonance position, O-mode injection and the higher B_z at the field-null centre, as evidenced by the D_α emission and the central ECE signal. The ECH is turned on at $t = -0.04$ s and the inductive voltage begins at $t = 0$ s. (*a*) is the ECH power, (*b*) is the H_α signals, (*c*) line-averaged plasma density, (*d*) is the ECE signal and (*e*) is the pre-fill gas pressure. The hydrogen gas pre-fill begins at $t = -0.7$ s and maintained for 0.1 s. The solid line (shot 833) is for the perpendicular EC beam launch crossing the equatorial plane at the resonance position for the conventional field configuration, the thin dashed line (shot 967) is for the perpendicular EC beam launch crossing the equatorial plane at the resonance position for the dipole-like field configuration, the thick dashed line (shot 974) is for the perpendicular and downward EC beam launch toward the lower position (∼−0.1 m) from the equatorial plane and the thick dashed–dotted line (shot 1057) is for the downward EC beam launch towards the lower position (∼−0.1 m) from the equatorial plane with toroidal angle of 10° in the direction opposite to the toroidal magnetic field. KSTAR is also operated with a TF field of 2 T at the major radius of 1.8 m which corresponds to the second harmonic resonant field with a 110 GHz EC wave. Figure 9 shows the CCD images and the temporal evolution of the plasma parameters for the shot with 110 GHz ECH-assisted startup using the second harmonic pre-ionization in the 2009 campaign.

3.3. Wall conditioning

A good initial vacuum and wall-conditioning procedure is essential to obtain a high-quality wall condition for plasma experiments. Various kinds of wall-conditioning techniques have been utilized to remove impurities from the surface of PFCs, including H_2O, carbon and oxygen compounds [20]. Wall conditioning in KSTAR mainly consists of baking, GDC, ICRH wall conditioning (ICWC) and boronization.

Various ICWC parameters have been scanned: pressure (He/H_2 mixture rate) and power coupling (CW, duty cycle). The response of the wall to the RF plasma is measured by RGA signals and emission spectroscopy. On the other hand, ICWC in between shots has been performed regularly during the campaign. Note that, because the TF field of the plasma shots was 2 T, no resonance layer was present in this case. Figure 10(*a*) shows numbers of molecules for masses M_2 and M_3 depending on the H_2 mixture rate. Using a night D_2 GDC, the wall was saturated by $\sim 10^{24}$ D atoms (similar to Tore Supra [21]). As He/H_2 ICWC is performed, the isotope exchange has occurred. The retention of H increases, as M_3 release increases. As the wall is saturated by H at 80 sccm, the H retention starts to decrease, thus production of HD also decreases. The number of $H_{\text{implanted}}$ is an order of $\sim 10^{21}$, while

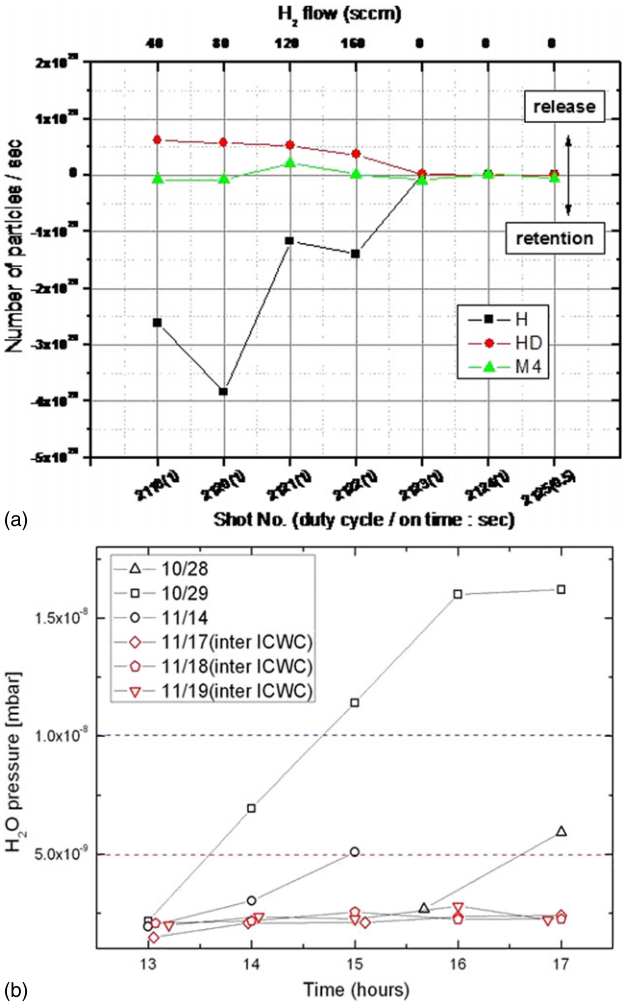

Figure 10. (*a*) Numbers of molecules of M_2 and M_3 depending on the H_2 mixture rate with a steady He flow. (*b*) Water removal by inter-shot ICWC during the campaign.

that of D_{pumped} is $\sim 10^{20}$ with a ratio of $H_{\text{implanted}}/D_{\text{pumped}} \sim 5$–15. The H retention rate is of the order of $\sim 10^{19}\,\text{H}\,\text{s}^{-1}$. It should be noted that we cannot separate D_2 and He by RGA. Nevertheless, the ICWC results from Tore Supra have shown that the D_2 partial pressure during the ICWC is small compared with that of HD ($\sim$10%) [22]. Thus, the estimated amount of D_{pumped} in the measurements would have about 10% of errors.

Figure 10(*b*) shows an example of the water removal by inter-shot ICWC. During the second campaign, water was the dominant impurity throughout with an average percentage of about 7%. Without Inter-shot ICWC, the water pressure increases rapidly over several hours up to 1.5×10^{-8} mbar. The increase in water pressure is effectively suppressed by inter-shot ICWC.

The operational windows for GDC have been scanned and the optimization is underway. In a He GDC, a particle removal rate of $\sim 10^{18}$–10^{19} particle s^{-1} is obtained while that of ICWC is $\sim 10^{17}$–10^{18} particle s^{-1}. The H removal rate of He ICWC ($\sim 10^{18}\,\text{H}\,\text{s}^{-1}$) is about 5–10% of that in GDC. The HT-7 and EAST showed an absolute H removal rate of $(1\text{–}4) \times 10^{19}\,\text{H}\,\text{s}^{-1}$ [23].

The ICWC results are consistent with those obtained in other machines. Pulsed operation seems more effective than continuous application. From the observation by the in-vessel TV system, it seems that the cleaning is effective at the low-field side of the wall. Also, the homogeneity of the plasma was improved by applying external poloidal magnetic fields.

First boronization in KSTAR was successfully performed using carborane vapour. Water and oxygen levels in vacuum vessel have been reduced significantly. However, additional H atoms dissociated from the carborane mother molecule would be a minor problem for the density control during the following shots. Boron containing thin film deposited by boronization is a hard diamond-like film with a small amount of boron components with a density of 2.0–2.2 $\text{g}\,\text{cm}^{-3}$, H/H+C ratio of 25–30%.

3.4. Dust characterization

Inner wall configuration of KSTAR is gradually upgraded through campaigns from metallic to full graphite wall. Dust is collected by dedicated dust collectors installed below the vertical ports, and by a vacuum cleaner with fine filters and sticky carbon tapes after the vent of the machine. Dust is analysed by SEM to obtain size distribution and by electron probe micro-analysis (EPMA) to identify the chemical composition. About 475 mg of the dust was collected by vacuum cleaner after the second campaign. Metallic dust collected after the second campaign would give additional information on ITER dust creation.

From the EPMA measurements of the dust, C, Fe, Cr, Ni, Cl, Au, Ag, Si were found (data not shown here). Dust with a size of several micrometres was made of metal pieces that have almost identical composition as vacuum vessel. Broken pieces of graphite were also observed. By analysing the size of the dust, two different size distributions were identified: one has a peak at 100 nm and the other at 2 μm. In general, dust created by flaking and brittle destruction has non-spherical shape while that created by arcing and volume polymerization has spherical shape. The presence of hydrogeneted carbon (a-C : H) nanoparticles of size smaller than 0.1 μm in diameter with a well-defined Gaussian size distribution within a certain full-width half maximum (FWHM) is identified in many machines equipped with graphite PFCs. This is clear evidence of plasma volume polymerization [24, 25] in fusion devices.

KSTAR is now contributing to the IAEA Coordinated Research Project on 'characterization of size, composition and origins of dust in fusion devices'. This project is to build up a dust database at IAEA which includes all possible information on the dust collected from tokamaks, and will be extended for dust from laboratory.

3.5. Observation of H-mode transition

In the 2010 campaign, the first H-mode discharge (shot 4200) in KSTAR was achieved as shown in figure 11. It was done on $B_{\text{T}} = 2.0\,\text{T}$ with $I_{\text{P}} = 0.6\,\text{MA}$ in a well-balanced double-null configuration ($\kappa_x \sim 1.8$, $\delta_x \sim 0.6$) after the boronization on the wall by carborane. The additional heating power was 1.4 MW NBI (80 keV co-injection) and 0.2 MW ECRH (counter), and the line-averaged density was about

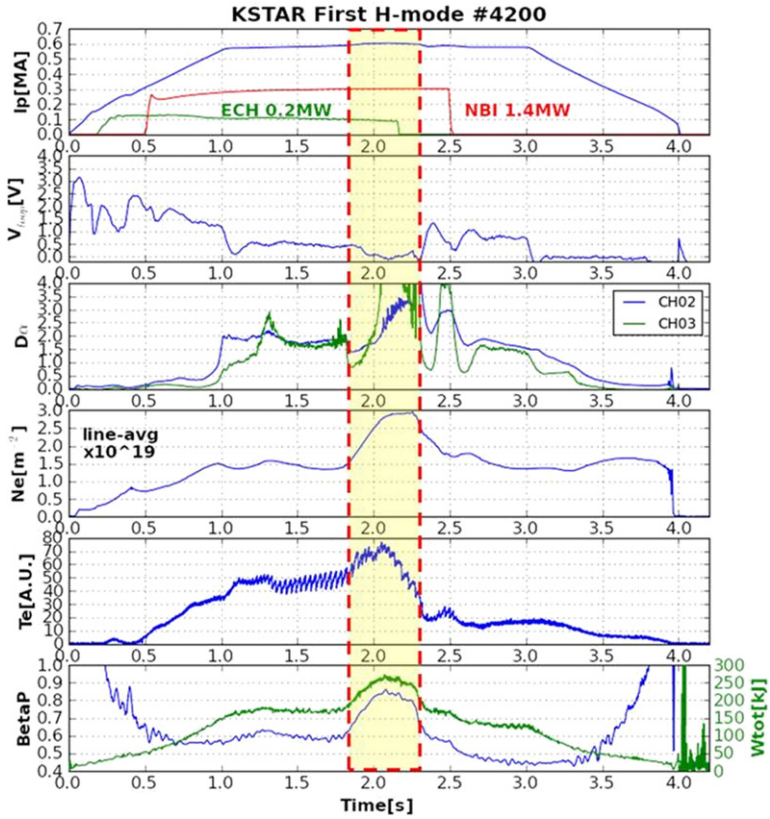

Figure 11. The first H-mode transition in KSTAR. Substantial increases of electron density and temperature, and stored energy are visible and ELM occurred in the D_α signal.

$1.5 \times 10^{19}\,\mathrm{m}^{-2}$. As shown in the figure, the plasma energy is doubled during the H-mode phase and it suggests the H_{89} factor is about two, like a typical H-mode discharge. H-mode was sustained about 0.5 s showing clear H–L back transition at 2.3 s. The increase in ion temperature during the L–H transition was also confirmed by the charge exchange spectroscopy (CES) and the x-ray imaging crystal spectroscopy (XICS) measurements. However, since the plasma shape control was not applied, the electron temperature started decreasing before the back transition occurred.

3.6. Analysis and prediction

Here, we introduce briefly some theoretical and simulation work performed for the experimental data analysis and operation scenario modeling of KSTAR over the last two years. Firstly, in relation to the ECH-assisted startup, an analytic study has been performed on the electron cyclotron resonance heating process in the first and second harmonic resonance cases [26, 27]. A net energy gain when particles go through a resonance zone was calculated using a collision-less nonlinear cyclotron heating model with a realistic wave beam profile. It is found that the axis and frequency of nonlinear energy-oscillation are about one order higher so that electrons can gain the energy up to several hundred eV in the first harmonic resonance case, while only up to $\sim$10 eV in the second harmonic one. Thus, ECH can heat up low-energy electrons of room temperature order to several hundred eV rapidly with the first harmonic resonance, while it takes a longer time for the second harmonic case. This theoretical model thus provides a qualitative explanation for the delay of pre-ionization time observed in the second harmonic ECH experiment as described in section 3.2.

A new theoretical model has also been developed to explain the observed plasma current during the ECH pre-ionization experiment, where a few hundred amperes was repeatedly measured even when the ECH beam was launched vertically to the toroidal magnetic field with no preferable toroidal direction [28]. Noting that the only factor breaking the toroidal symmetry is a tiny vertical magnetic field within the field-null region, and the average life time becomes different between the electrons flying to clockwise or counter-clockwise when the vertical motion due to this small field combines with the grad-B drift, an analytic calculation was done to obtain a finite ECH driven electron current for a given density, temperature and vertical magnetic field. It is found that the calculated current is well within the order of the experimental observation, thus providing another explanation different from the previous model by Forest *et al* [29], where the ECH driven current was explained by the Pfirsh–Schluter, bootstrap and precession-drift current models.

In relation to the KSTAR divertor experiment with the D-shape plasmas, a two-dimensional simulation study has also been made of the transport of divertor plasmas in the KSTAR model using the B2.5 code [30]. Maximal divertor heat fluxes were evaluated in the sheath-limited regime at various powers, and the effect of C impurities on the divertor heat flux was investigated. It is shown that the C impurities change the

Table 2. Schedule of the KSTAR operation and system upgrade for the initial five years.

Campaign	2008	2009	2010	2011	2012
Operation Time	'08. 3 ~'08. 8	'09. 8 ~'09.12	'10.6 ~'10.12	'11. 4 ~'11. 9	'12. 3 ~'12. 8
Experimental goals	• First plasma startup • 2nd Harmonic ECH pre-ionization	• Startup stabilization • ECH pre-ionization • ICRF wall conditioning	• Shape control • L-mode • MHD study • Wall conditioning	• H-mode • MHD • Disruption • Wall interaction	• Profile control • ITER shape • ELM & disruption
Operation Parameters	• B_T ~ 1.5 T • I_P > 0.1 MA • t_p > 0.1 s • Te ~ 0.3 keV • Shape ~ Circular • Gas : H_2	• B_T : 2 ~ 3.5 T • I_P > 0.3 MA • t_p > 2 s • Te ~ 1 keV • Shape ~ Circular • Gas : D_2	• B_T : 2 ~ 3.5 T • I_P > 0.5 MA • t_p > 5 s • Ti ~ 1 keV • Shape ~ DN (κ2.0) • Gas : D_2	• B_T : 2 ~ 3.5 T • I_P > 1 MA • t_p > 10 s • Ti ~ 3 keV • Shape ~ DN & SN • Gas : D_2	• B_T : 2 ~ 3.5 T • I_P > 1 MA • t_p ~ 20 s • Ti ~ 5 keV • Shape ~ DN & SN • Gas : D_2
Magnetic Control	• TF : 15 kA [1.5T) • PF : 4 kA (~1 Wb) • Grid : 50 MVA	• TF : 35 kA [3.5 T] • PF : +/-4 kA (~2 Wb) • Grid : 50 MVA	• TF : 35 kA [3.5 T] • PF : +/-10 kA (~4 Wb) • IVCC : VS • Grid: 100 MVA	• TF : 35 kA [3.5 T] • PF : +/-15 kA (~6Wb) • IVCC : VS • Grid: 100 MVA	• TF : 35 kA [3.5 T] • PF : +/-20 kA (~8Wb) • IVCC : FEC,RMP,RWM • Grid: 100 MVA
Vacuum Conditioning	• Inboard limiter (belt) • Gas puff • Glow DC	• Inboard limiter + Boronization + ICRF DC	+ Divertor + Passive stabilizer + In-vessel coil + PFC baking	+ PFC cooling	+ Cryopump operation
Heating & Current Drive	• ECH(84G):0.3MW, 0.4s	• ECH(110G): 0.2MW, 2s • ICRH: 0.3MW, 1s	• ECH(110G): 0.5MW • ICRH: 1MW • NBI: 1MW	• ECH(84/110G): 0.5MW • ECCD(170G): 1MW • ICRH : 1.5MW • NBI: 2MW • LHCD: 0.3MW	• ECH(84/110G): 0.5MW • ECCD(170G): 1MW • ICRH : 1.5MW • NBI : 5MW • LHCD : 0.3MW
Diagnostics	• Magnetic Diagnostics/ MMWI / ECE / Hα / VS / filterscope / TV / • Hall probe array	+ XICS / Soft X-ray / Hard X-ray/ Resistive Bolometer / Probe / Reflectometer • e-beam	+ Thomson/ ECEI/ IRTV / Image Bolometer/ CES / neutron / XICS-2 / Ellipsometry /	+ FIR / Div. bolometer / X-ray pinhole / Coherence Imaging/ fast-ion / etc	+ MSE / MIR / BES / VUV / CX-NPA /etc

intensive radiation position from the outer SOL region near the divertor to a private region near the X-point, and the radiation near the X-point gives rise to effective removal of the peak heat flux. The change in the intensive radiation position appears to induce an increase in the heat influx to the private region from the SOL region across the separatrix, resulting in a significant reduction in the divertor heat flux near the striking point.

Finally, a detailed analysis has been done for the ideal MHD stability limit of the KSTAR target AT modes [31]. For a set of model equilibria with the reverse-shear q-profile the stability boundaries of the low-n external kink modes were calculated using the two codes of DCON and GATO. It is found that the dependence of the β_N limit on the toroidal mode number n changes significantly with the pressure profile. In the relatively peaked profile, the β_N limit increases with n, so that the possible maximum β_N is almost decided by the $n = 1$ mode. Meanwhile, in the cases with a broader pressure profile, the β_N limit decreases with n, making the maximum β_N determined by higher n modes ($n = 3$, here). With this change in the mode number of the most unstable mode, the maximum β_N value appears to decrease substantially as the pressure profile becomes broader.

4. Summary and near-term plan

In this report we have presented detailed results of machine upgrade and experimental research in KSTAR for the earlier phase of operations. As was predicted in [32], with the planned heating and CD systems in a couple of years, it is expected that most of the important features of the steady-state, AT mode of operation can be achieved in KSTAR; fully non-inductive, high performance, high confinement, high bootstrap current fraction and keeping these features for longer pulse duration. Other features which cannot be considered easily for the simulation work, such as the optimized operation of the liquid-He facility, better particle control, efficient power exhaust and active suppression of MHD modes with reliable actuators and control systems should also be prepared and practiced reliably.

Summarizing some of the major results, first for the machine upgrade, all of the PFCs, which include an inboard limiter, divertor and passive stabilizer, have been installed inside the vacuum vessel. The sixteen segmented IVCCs were also installed between the PFCs and the vacuum vessel. In addition, the first NBI system (NBI-1), designed to deliver 8 MW deuterium neutral beams into the KSTAR plasmas with three ion sources, was installed and tested. In addition, substantial upgrades have been made in diagnostics, control, power supply and other heating/CD systems.

For the experimental research, after the first plasma experiment in 2008, the second and third campaigns were carried out. Ohmic plasma current was ramped-up over 700 kA with the pulse length of more than 7 s. Toroidal field was applied up to 3.6 T, exceeding the design limit of 3.5 T. Substantial progress has been made in resolving the startup issues, particularly related to the stray field caused by the Incoloy 908 magnetic material in superconducting coils and the eddy current by the up-down asymmetric cryostat structure. The ECH-assisted startup scenarios with a relatively low loop voltage of about 2 V were established well with the second harmonic pre-ionization using 84 GHz/350 kW and 110 GHz/250 kW gyrotrons at the toroidal field of 1.5 T and

2 T, respectively. Plasma control using feed-forward and feedback routines was successfully applied for producing circular plasmas. The IVCC has been used for vertical position control to produce shaped plasmas, obtaining highly elongated ($\kappa \sim 1.9$, $\delta \sim 0.8$) plasmas. The first H-mode transition was observed with NBI and EC heating for elongated plasmas with a relatively good wall condition. Several wall-conditioning methods, such as GDC, ICWC, boronization and baking were tested and now have been routinely utilized. The study of dust particles was also started using dust collectors and coupons, establishing a valuable database.

For the next campaign a main target is to obtain the H-mode plasma reliably and to understand it better. Table 2 shows the first five-year plan of the KSTAR experimental campaign and the facility upgrade. The heating power will be upgraded to about 5 MW, which is estimated to be above the H-mode threshold value in most of the KSTAR operation windows. Diagnostics will also be upgraded for the measurement of plasma properties near the pedestal and divertor region. The initial study will then be performed to understand the basic characteristics and physics of H-mode plasma, such as the energy confinement time, L–H transition, pedestal, plasma rotation and ELM control. In the coming years the plasma current will also be increased up to 1 MA with a pulse length of about 10 s, targeting to reach up to 2 MA with a pulse length of 20 s in the pure ohmic mode and more detailed physics studies will be made of MHD instability, plasma heating and plasma-wall interaction issues. The research of H-mode plasma will be continued, focusing more on a detailed physics study in a high toroidal magnetic field of up to 3.5 T. For this, the diagnostic system will be upgraded substantially, particularly to implement the advanced turbulence measurement systems, such as MIR and BES. The active control of ELM as well as FEC will also be possible through the upgrade of the IVCC power supply system. The high-field-side pellet injection system will also be available for the study of particle transport and density profile control. A study of current-drive experiment will also be performed of the current profile control using NBCD, ECCD and LHCD systems, targeting for full non-inductive, steady-state operation which will be the main research area for the next operation period of KSTAR.

Acknowledgments

The authors thank all of the technical and administrative staff to run the KSTAR program flawlessly and smoothly. The authors also thank M. Kikuchi and K. Ida for their effort in the internal review and for providing valuable comments. This work was possible by the close collaboration with many domestic and international institutes and their active and collaborative participation to the KSTAR program. The authors thank the officers in the administration and international affairs offices of all of the participating institutes for their role in making an environment where the practical collaboration happened. This work was supported by the Ministry of the Education, Science and Technology of Korea.

References

[1] Oh Y.K. *et al* 2009 *Fusion Eng. Des.* **84** 344–50
[2] Tsitrone E. 2007 *J. Nucl. Mater.* **363–365** 12–23
[3] Hong S.H. *et al* 2010 First boronization in KSTAR *Fusion Eng. Des.* **85** 946–9
[4] Hong S.H. *et al* 2011 Initial phase wall conditioning in KSTAR *Nucl. Fusion* submitted
[5] Park S.H. *et al* 2010 *Proc. 23rd Int. Conf. on Fusion Energy 2010 (Daejeon, Korea, 2010)* (Vienna: IAEA) CD-ROM file FTP/P6-28 and http://www-naweb.iaea.org/napc/physics/FEC/FEC2010/html/index.htm
[6] Park Y.S. *et al* 2011 KSTAR Equilibrium operating space and projected stabilization at high normalized beta *Nucl. Fusion* **51** 053001
[7] Lee G.S. *et al* 2001 *Proc. ITC-10 (Toki, Japan, 2001)* and http://www.nifs.ac.jp/itc/itc10/index.html
[8] Jhang H., Kessel C.E., Pomphrey N., Kim J.-Y., Jardin S.C. and Lee G.S. 2001 *Fusion Eng. Des.* **54** 117–34
[9] Kim D. *et al* 2010 *Plasma Phys. Control. Fusion* **52** 095009
[10] Kim H.K. *et al* 2009 *Fusion Eng. Des.* **84** 1029–32
[11] Jeong S.H. *et al* 2008 *Rev. Sci. Instrum.* **79** 02B310
[12] Bae Y.S. *et al* 2009 *Nucl. Fusion* **49** 022001
[13] Hoang G.T. *et al* 2009 *Nucl. Fusion* **49** 075001
[14] Park S. *et al* 2010 *Fusion Eng. Des.* **85** 197–204
[15] Kim W.C. *et al* 2010 *Proc. 23rd Int. Conf. on Fusion Energy 2010 (Daejeon, Korea, 2010)* (Vienna: IAEA) CD-ROM file PD/P1-2 and http://www-naweb.iaea.org/napc/physics/FEC/FEC2010/html/index.htm
[16] Yoon S.W. *et al* 2010 *Proc. 23rd Int. Conf. on Fusion Energy 2010 (Daejeon, Korea, 2010)* (Vienna: IAEA) CD-ROM file EXS/5-1 and http://www.naweb.iaea.org/napc/physics/FEC/FEC2010/html/index.htm
[17] England A.C. *et al* 2011 *Fusion Eng. Des.* **86** 20–6
[18] Jeon Y.M. *et al* 2010 *Proc. 23rd Int. Conf. on Fusion Energy 2010 (Daejeon, Korea, 2010)* (Vienna: IAEA) CD-ROM file EXS/P5-08 and http://www.naweb.iaea.org/napc/physics/FEC/FEC2010/html/index.htm
[19] Portone A. *et al* 2008 *Fusion Eng. Des.* **83** 1619
[20] Winter J. 1996 *Plasma Phys. Control. Fusion* **38** 1503–42
[21] Douai D., Wauters T., Bremond S., de la Cal E., Lombard G., Lyssoivan A., Pergourie B., Tsitrone E. and Tore Supra Team, Special Expert Working Group on Fuel Removal 2009 private communication
[22] Douai D. *et al* 2010 *J. Nucl. Mater.* at press doi: 10.1016/j.jnucmat.2010.11.083
[23] ITPA Div/SOL Group, private communication *12th ITPA Div/SOL Group Meeting Report*
[24] Hong S. 2004 From thin films to nanoparticles: investigation of polymerization processes in capacitively coupled hydrocarbon plasmas *PhD Thesis* Ruhr-University Bochum, Bochum, Germany
[25] Hong S.-H., Murari A., Loarer T., Huber A., Grisolia C., Monier-Garbet P., Winter J. and JET EFDA contributors, EFDA–JET–PR(09)24
[26] Seol J.-C., Hegna C.C. and Callen J.D. 2009 *Phys. Plasmas* **16** 052512
[27] Seol J.-C., Park B.H., Kim S.S., Kim J.Y. and Na Y.-S. 2010 *Nucl. Fusion* **50** 105008
[28] Park B.H. *et al* 2010 *37th EPS Conf. on Plasma Physics (Dublin, Ireland, 2010)* vol 34A (ECA) p P-5.174
[29] Forest C.B., Hwang Y.S., Ono M. and Darrow D.S. 1992 *Phys. Rev. Lett.* **68** 3559
[30] Kim S.S., Yoon S.W. and Kim J.Y. 2010 *J. Korean Phys. Soc.* **56** 1119
[31] Yi S., Kim J.Y. and Ryu C.M. 2010 *Fusion Eng. Des.* **85** 796
[32] Na Y.S. *et al* 2009 *Nucl. Fusion* **49** 115018